IEEE Access
Multidisciplinary ⋮ Rapid Review ⋮ Open Access Journal

Received 4 September 2023, accepted 14 September 2023, date of publication 28 September 2023,
date of current version 5 October 2023.

Digital Object Identifier 10.1109/ACCESS.2023.3320108

RESEARCH ARTICLE

Novel Chipless RFID Tags Using Eight State Triple-Mode Resonators

ENGIN DOGAN[1], (Student Member, IEEE), ALI KURSAD GORUR[2], (Member, IEEE), AND ADNAN GORUR[1]

[1]Department of Electrical-Electronics Engineering, Niğde Ömer Halisdemir University, 51240 Niğde, Turkey
[2]Department of Electrical-Electronics Engineering, Nevşehir Haci Bektaş Veli University, 50300 Nevşehir, Turkey

Corresponding author: Ali Kursad Gorur (akursadgorur@hotmail.com)

This work was supported by the Scientific and Technological Research Council of Turkey (TÜBİTAK) under Grant 119E476.

ABSTRACT For multi-resonator based chipless radio frequency identification (RFID) tags, a novel triple-mode resonator is designed by loading open-circuited stubs to a transmission line which is coupled to input and output ports. Since the proposed resonator provides independently controllable three resonant frequencies, three bits can be obtained by means of a single triple-mode resonator. The presence and absence of the open stubs results in eight states from a single triple-mode resonator. Therefore, N triple-mode resonators in different lengths can generate 8^N different frequency codes. For this purpose, a multi-resonator circuit operating between 1.9 and 3.75 GHz is also developed by using 5 triple-mode resonators, so that 15 resonant frequencies can be obtained. Two conventional vertically/horizontally polarized monopole antennas are used to demonstrate the tag performance. Bit density and spectral efficiency of the designed tag are 29.04 bits/ λ_g^2 and 8.33 bits/GHz. Two chipless RFID tags having different frequency codes have been fabricated and tested in a good agreement with the predicted results. The designed tags have also been tested under various circumstances successfully.

INDEX TERMS Chipless, eight state, monopole antenna, RFID tag, triple-mode resonator.

I. INTRODUCTION

In recent years, the utilization of radio frequency identification (RFID) tags for item tracking applications has dramatically increased. Although they could still not replace the barcodes, they are expected to increase their popularity in the following years due to their advantages such as longer reading distance and line of sight. There are two types of RFID tags: Chipped and chipless tags. The chipped RFID tags can achieve the encoding process by virtue of the identification number of the chip. In contrast, chipless RFID tags generate different identification numbers or codes depending on the circuit topology. Therefore, developing new chipless RFID circuits that allow a high number of codes within a compact size is crucial.

Chipless RFID tags are examined under three main headlines as time-domain reflectometry, amplitude/phase backscatter modulation, and spectral signature. Time-domain reflectometry based chipless RFID tags especially use surface acoustic wave resonators and data encoding process is performed by partial reflections from the tag [1], [2], [3], [4], [5], [6]. The second type is amplitude/phase backscatter modulation based chipless RFID tags that can achieve data encoding process through the amplitude or phase of the backscattered signal [7], [8], [9], [10], [11], [12]. Although they can be produced cost-effectively and allow for long reading distances, they especially suffer from the bit capacity. Therefore, they are not as preferable as spectral signature based chipless RFID tags in industrial fields that require a high item tracking capacity. Spectral signature based chipless RFID tags encode data depending on their frequency responses. These tags receive the interrogation signal from reader, and the signal is backscattered after the encoding process. The encoding is performed by a multi-resonant circuit on the tag.

Spectral signature based chipless RFID tags behave as transceivers since they both receive and transmit signals. They can be categorized into two types: With and without

The associate editor coordinating the review of this manuscript and approving it for publication was Giorgio Montisci.

antennas. Tags without antennas act like a scatterer, and their coding process is performed through Radar Cross Section (RCS) results. Such tags can be constructed using open loop resonators [13], [14], [15], [16], [17], [18] and slots [19], [20], [21], [22], [23], [24]. The resonator types discussed in these studies produce a single resonance, which means only 2 codes can be produced for the tag [19], [20], [21], [22], [23], [24]. In order to increase the number of codes, a frequency shifting technique is employed [16], [17], [18]. However, this process relatively occupies a high frequency range. On the other hand, tags with antennas can either integrate the antenna with the multi-resonant circuit [25], [26], [27], [28], [29], [30], [31] or two monopole antennas in vertical/horizontal polarizations for receiving or transmitting processes [32], [33], [34], [35]. Tags with integrated antennas can be designed as a single part, which includes the monopole antennas and the multi-resonator circuit. These tags are advantageous due to their compact circuit size and low cost. The coding process is carried out over the transmission coefficient, S_{21}, between the transmitter and receiver antennas of the reader. While both phase and amplitude variations of the transmission coefficient at resonant frequencies can be used for encoding [36], the presence of resonant frequencies is more favored for encoding, as the bits can be detected more easily. From this view of point, multi-resonator circuits have a significant place for the tags integrated with antennas since they determine the coding variety within a compact circuit size. Therefore, there is a need to develop new resonator configurations for chipless RFID tags to achieve high code density and further miniaturization of the tag size. The resonator configurations coupled to a straight feeding line that connects receiver and transmitter monopole antennas determine the bit capacity. For example, a single open loop resonator can produce two states, allowing for 2^N frequency codes using N open loop resonators [35]. To date, such resonators have been studied by various researchers especially in spiral structures for size reduction [25], [26]. In order to increase the number of states, dual-mode resonators have been used to obtain two resonant frequencies from a single resonator. Thus, three and four states have been observed depending on the placement of the resonator [30], [31], [32], [33]. In addition to dual-mode resonators, triple-mode resonators that exhibit 5 states have also been introduced for chipless RFID tags to achieve more states [37]. Although more than 5 states can be obtained in [16] and [18], the encoding process is realized through phase deviation and frequency adjustments. Therefore, these tags can be developed to provide much more frequency codes by using multi-mode resonators. To the best of our knowledge, no one has achieved more than 5 states from a single resonator to date.

In this paper, a novel triple-mode resonator constructed by loading stepped impedance stubs is introduced. The proposed resonator enables the switching and control of all the resonant frequencies. Hence, each resonant frequency can be independently cancelled. Based on the proposed resonator, three resonant frequencies are considered as three bits, and totally eight states can be achieved from a single resonator. Thus, in case of using N triple-mode resonators, 8^N different frequency codes can be observed. For demonstration purposes, a multi-resonator circuit consisting of five triple-mode resonators coupled to the transmission line connecting the input and output ports is designed. Two conventional monopole antennas as receiver and transmitter instead of input and output ports are used for constructing a complete chipless RFID tag architecture. The designed tags exhibit 15 resonant frequencies within the 2-4 GHz frequency range. Two chipless RFID tags having different frequency codes have been manufactured and successfully tested.

This paper is organized as follows. Analytical expressions for an asymmetrically coupled single triple-mode resonator are introduced in Section II. This section also discusses theoretical frequency responses and coding process. Section III describes the construction of the proposed eight state chipless RFID tags. Additionally, this section investigates the conventional monopole antenna and provides simulated frequency responses of the multi-resonator circuit. Experimental studies and significance of the proposed tags are discussed in Section IV.

II. EIGHT STATE TRIPLE-MODE RESONATORS

As described previously, multi-resonator circuits based chipless RFID tags can encode signals due to the existence of resonant frequencies. Since these circuits behave like bandstop filters, the resonant frequencies are also the transmission zeros. Hence, a bit of logical '0' can be represented by a transmission zero, whereas a logical '1' can be represented by cancelling the zero. In order to design a multi-resonator circuit, the proposed triple-mode resonator is firstly characterized by using the asymmetrical coupled line theory, as introduced in [38].

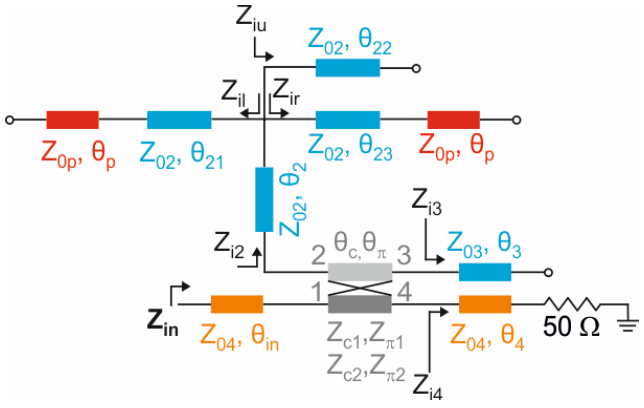

FIGURE 1. Equivalent circuit model of the single triple-mode resonator coupled to input and output ports.

A. ANALYSIS OF COUPLED TRIPLE-MODE RESONATOR

The equivalent circuit model of the proposed triple-mode resonator, coupled to a straight transmission line between

input and output ports, is depicted in Fig. 1. The straight transmission line can also be referred to as the feeding line since it feeds the resonator. For a comprehensive analysis, the coupled section between the resonator arm and the feeding line is considered as asymmetrical so as to have unequal line widths. As can be seen from the figure, the proposed resonator is constructed using stepped impedance open-circuited stubs and located horizontally for appropriate coupling mechanism. Therefore, the equivalent circuit model has also asymmetry and the analysis can be performed by calculating the input impedance as,

$$Z_{in} = Z_{04}\frac{Z_T + jZ_{04}\tan(\theta_{in})}{Z_{04} + jZ_T\tan(\theta_{in})} \tag{1}$$

where, Z_{04} and θ_{in} are the characteristic impedance and electrical length of the transmission line at the input, respectively. Also, Z_T is the load impedance at the first port of the coupled section. This can be found by asymmetrical coupled line analysis [38], [39]. The current and voltage expressions of a four-port network can be written as,

$$V_1 = I_1Z_{11} + I_2Z_{12} + I_3Z_{13} + I_4Z_{14} \tag{2a}$$
$$V_2 = I_1Z_{21} + I_2Z_{22} + I_3Z_{23} + I_4Z_{24} \tag{2b}$$
$$V_3 = I_1Z_{31} + I_2Z_{32} + I_3Z_{33} + I_4Z_{34} \tag{2c}$$
$$V_4 = I_1Z_{41} + I_2Z_{42} + I_3Z_{43} + I_4Z_{44} \tag{2d}$$

The impedance matrix elements of the four port asymmetrical network can be calculated using the following set of equations [38].

$$Z_{11} = Z_{44} = \frac{Z_{c1}\coth(j\theta_c)}{1 - R_c/R_\pi} + \frac{Z_{\pi 1}\coth(j\theta_\pi)}{1 - R_\pi/R_c} \tag{3a}$$
$$Z_{12} = Z_{21} = \frac{Z_{c1}R_c\coth(j\theta_c)}{1 - R_c/R_\pi} + \frac{Z_{\pi 1}R_\pi\coth(j\theta_\pi)}{1 - R_\pi/R_c} \tag{3b}$$
$$Z_{13} = Z_{31} = \frac{Z_{c1}R_c}{(1 - R_c/R_\pi)\sinh(j\theta_c)} + \frac{Z_{\pi 1}R_\pi}{(1 - R_\pi/R_c)\sinh(j\theta_\pi)} \tag{3c}$$
$$Z_{14} = Z_{41} = \frac{Z_{c1}}{(1 - R_c/R_\pi)\sinh(j\theta_c)} + \frac{Z_{\pi 1}}{(1 - R_\pi/R_c)\sinh(j\theta_\pi)} \tag{3d}$$
$$Z_{22} = Z_{33} = -\frac{R_cZ_{c2}\coth(j\theta_c)}{R_\pi(1 - R_c/R_\pi)} - \frac{R_\pi Z_{\pi 2}\coth(j\theta_\pi)}{R_c(1 - R_\pi/R_c)} \tag{3e}$$
$$Z_{23} = Z_{32} = \frac{R_c^2Z_{c1}}{(1 - R_c/R_\pi)\sinh(j\theta_c)} + \frac{R_\pi^2Z_{\pi 1}}{(1 - R_\pi/R_c)\sinh(j\theta_\pi)} \tag{3f}$$

In (3a)-(3f), θ_c and θ_π represent the electrical lengths for the c- and π- mode equivalent circuits, respectively. R_c and R_π are the voltage ratios on the asymmetrical transmission lines to be used for calculating the characteristic impedances of the c- and π- modes.

As shown in Fig. 1, the input voltages of the four-port network are $V_2 = -I_2Z_{i2}$, $V_3 = -I_3Z_{i3}$, and $V_4 = -I_4Z_{i4}$. Using these conditions in (2), the voltage-current relation at the first port of the coupled section can be expressed with the following set of equations.

$$Z_T = \frac{V_1}{I_1} = Z_{11} + NZ_{12} + MZ_{13} + \frac{LZ_{14}}{K} \tag{4}$$
$$K = 1 - \frac{Z_{24}Z_{42}}{AC} - \frac{(AZ_{43} + Z_{32}Z_{42})^2}{ACD} \tag{5a}$$
$$L = \frac{Z_{41}A + Z_{42}Z_{21}}{AC} + \frac{(AZ_{42} + Z_{21}Z_{32})(Z_{31}Z_{23} + AZ_{43})}{ACD} \tag{5b}$$
$$M = \frac{Z_{31}A + Z_{21}Z_{32}}{D} + \frac{LZ_{34}A + LZ_{32}Z_{24}}{KD} \tag{5c}$$
$$N = \frac{Z_{21}}{A} + M\frac{Z_{23}}{A} + \frac{LZ_{24}}{KA} \tag{5d}$$

where, A, B, C and D can be simplified as,

$$A = -(Z_{i2} + Z_{22}) \tag{6a}$$
$$B = -(Z_{i3} + Z_{33}) \tag{6b}$$
$$C = -(Z_{i4} + Z_{44}) \tag{6c}$$
$$D = AB - Z_{23}^2. \tag{6d}$$

Here, Z_{i2} is the input impedance seen from the second port of the coupled section and can be expressed as,

$$Z_{i2} = Z_{02}\frac{Z_{i2L} + jZ_{02}\tan(\theta_2)}{Z_{02} + jZ_{i2L}\tan(\theta_2)} \tag{7}$$

where Z_{i2L} is the equivalent impedance of the Z_{il}, Z_{iu} and Z_{ir} as shown in Fig. 1 and can be calculated from the following equations.

$$Z_{i2L} = Z_{il}//Z_{iu}//Z_{ir} \tag{8a}$$
$$Z_{il} = Z_{02}\frac{ZL_{21} + jZ_{02}\tan(\theta_{21})}{Z_{02} + jZL_{21}\tan(\theta_{21})} \tag{8b}$$
$$Z_{iu} = -jZ_{02}\cot(\theta_{22}) \tag{8c}$$
$$Z_{ir} = Z_{02}\frac{ZL_{23} + jZ_{02}\tan(\theta_{23})}{Z_{02} + jZL_{23}\tan(\theta_{23})} \tag{8d}$$

where ZL_{21} and ZL_{23} represent the open-ended patch lines with electrical length of θ_p located at the end of the stubs. These stubs generate the first and third resonant frequencies of the resonator. As can be seen from Fig. 1, these impedances are equal to each other and can be expressed as,

$$ZL_{21} = ZL_{23} = -jZ_{0p}\cot(\theta_p). \tag{9}$$

In (6), Z_{i3} and Z_{i4} are the input impedances seen from the third and fourth ports of the coupled section shown in Fig. 1.

$$Z_{i3} = -jZ_{03}\cot(\theta_3) \tag{10a}$$
$$Z_{i4} = Z_{04}\frac{Z_0 + jZ_{04}\tan(\theta_4)}{Z_{04} + jZ_0\tan(\theta_4)} \tag{10b}$$

where $Z_0 = 50\ \Omega$ is the characteristic impedance of the output port. In (8), the electrical lengths of θ_{21}, θ_{22} and θ_{23}

may be represented by βd_{21}, βd_{22}, and βd_{23}, where d_{21}, d_{22} and d_{23} are the physical lengths of the related transmission lines. Three resonant frequencies can be obtained by means of these electrical lengths. Hence, it is possible to achieve three resonant frequencies in the presence of these transmission lines.

B. CODING PROCESS AND LAYOUT CONSTRUCTION

In order to encode the signal, the transmission coefficient of the two-port circuit needs to be investigated. Transmission zeros correspond to the '0' bit, whereas transmission at a specified frequency or frequency band is represented by logical '1'. Therefore, the locations of the transmission zeros determine the encoding process. In other words, transmission zeros can also be referred to as bit or resonant frequencies. As is well known, the reflection and transmission coefficients can be found by using (1) [40],

$$S_{11} = \frac{Z_{in} - Z_0}{Z_{in} + Z_0} \tag{11a}$$

$$|S_{21}| = \sqrt{1 - (|S_{11}|)^2} \tag{11b}$$

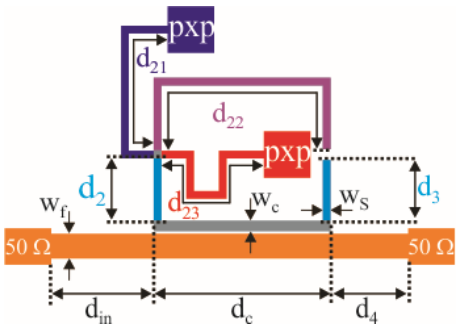

FIGURE 2. Layout of the proposed coupled triple-mode resonator.

Based on the equivalent circuit model given in Fig. 1, a triple-mode resonator asymmetrically coupled to input/output ports can be constructed, as shown in Fig. 2. In order to find the dimensions, the bit frequencies are firstly decided and then normalized with respect to the middle bit frequency. For example, in order to obtain bit frequencies at 2.73, 2.85 and 2.96 GHz, the normalized bit frequencies are calculated as 0.96, 1 and 1.04. After that, the wavelengths for each transmission line can be determined by seeking the normalized bit frequencies. Thus, the physical lengths in wavelength can be theoretically obtained as $d_2 = 0.052\lambda_m$, $d_{21} = 0.165\lambda_m$, $d_{22} = 0.243\lambda_m$, $d_{23} = 0.143\lambda_m$, $d_3 = 0.052\lambda_m$, $d_4 = 0.065\lambda_m$, $d_c = 0.147\lambda_m$, $d_{in} = 0.085\lambda_m$ and $p = 0.040\lambda_m$, where λ_m is the wavelength at the middle bit frequency of 2.85 GHz. The characteristic impedances shown in Fig. 1 are $Z_{c1} = 43.595$, $Z_{\pi 1} = 85.956$, $Z_{c2} = 59.133$ and $Z_{\pi 2} = 116.591$. The effects of d_{21}, d_{22}, and d_{23} on the normalized frequency responses are depicted in Figs. 3a, 3b, and 3c, respectively. The first bit frequency can be shifted to lower frequencies by increasing d_{21}, as shown in Fig. 3a. It should be noted that the second bit frequency is slightly affected by d_{21}, whereas the third one remains relatively unchanged. It is clear that the second bit frequency is mainly affected by d_{22}, while the first and third bit frequencies are only slightly affected by it, as shown in Fig. 3b.

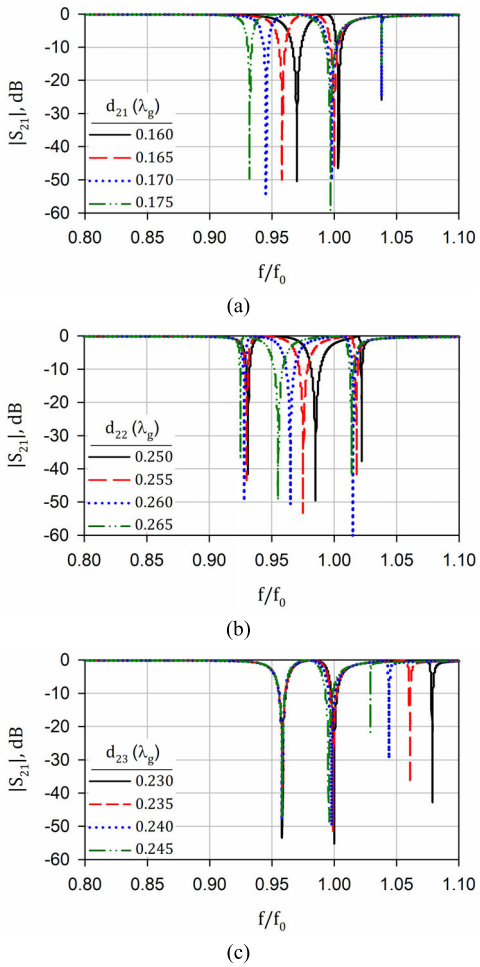

FIGURE 3. Adjustments of the bit frequencies with respect to the changes in a) d_{21}, b) d_{22} and c) d_{23}.

However, the third bit frequency can be independently controlled by changing d_{23} as shown in Fig. 3c. Thus, the third bit frequency affected by d_{22} can be shifted to the desired frequency by readjusting d_{23}. The first bit frequency can be kept fixed with respect to the changes in d_{23}. Accordingly, different frequency codes can be generated by eliminating the related bit. Since there are three independently controllable/switchable bits, totally $2^3 = 8$ states can be achieved from a single resonator.

The physical lengths can be found by calculating the wavelength at the middle bit frequency as,

$$\lambda_m = \frac{c}{f_m \sqrt{\varepsilon_{eff}}} \tag{12}$$

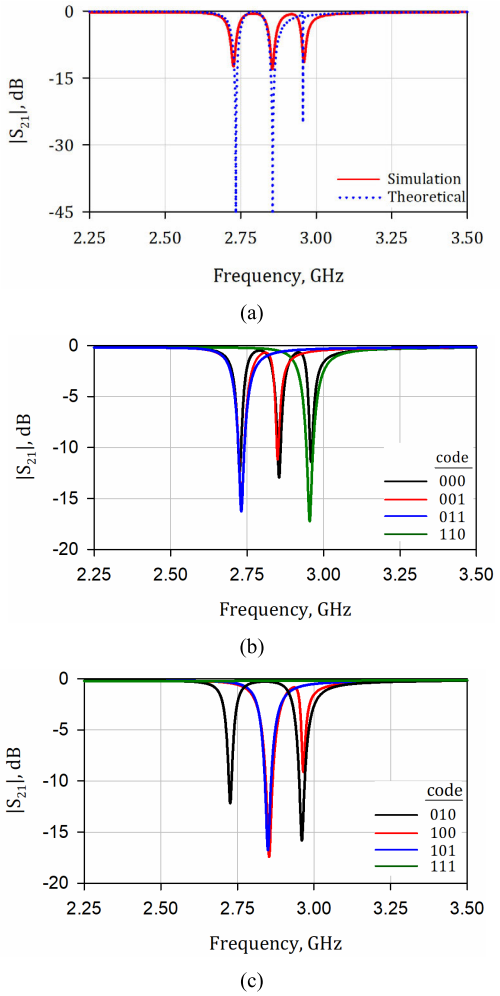

FIGURE 4. Proposed triple-mode resonator a) simulated and theoretical frequency responses. Frequency response representing different states of, b) 000 001, 011, and 110, c) 010, 100, 101, and 111.

where c is the speed of light, f_m is the middle bit frequency, and ε_{eff} is the effective dielectric constant of the related transmission line. Rogers RT5870 substrate with a dielectric constant of 2.33 and a thickness of 0.79 mm is used. Thus, all dimensions can be found as $d_2 = 4.00$, $d_{21} = 12.75$, $d_{22} = 18.80$, $d_{23} = 11.05$, $d_3 = 4.00$, $d_4 = 4.90$, $d_c = 11.30$, $d_{in} = 6.40$, and $p = 2.95$ mm. The frequency responses obtained from the theoretical analysis and the Full-Wave Electromagnetic Simulator (Sonnet) are shown in Fig. 4a. It should be noted that d_{21}, d_{22}, and d_{23} are bended to achieve a compact circuit size and the discontinuities are neglected in the mathematical equivalent circuit model. Therefore, after determining the dimensions theoretically, minor optimizations may be necessary for achieving better insertion loss levels at the desired bit frequencies. After the optimizations, the final dimensions shown in Fig. 2a can be extracted as $d_2 = 4.00$, $d_{21} = 12.40$, $d_{22} = 19.10$, $d_{23} = 10.95$, $d_3 = 4.00$, $d_4 = 4.90$, $d_c = 11.30$, $d_{in} = 6.40$, and $p = 2.95$ mm. Furthermore, the simulated frequency codes for 8 different states are illustrated in Figs. 4b and 4c. It is clear that all states can be achieved by eliminating the stubs, d_{21}, d_{22}, or d_{23}. When all of the stubs are included in the triple-mode resonator, three resonant frequencies can be observed. In other words, each stub can produce a single resonant frequency. Therefore, one can obtain one or two resonant frequencies by using just one or two of these stubs. In the absence of the stubs, the length of the remaining resonator will be shorter, meaning the resonant frequency will occur at higher frequencies than the desired frequency range. It means that no bit will be observed within the interested frequency range. By using the proposed approach, a single triple-mode resonator can meet the requirement of three open loop resonators of different lengths for three resonant frequencies. Hence, more compact multi-resonator circuits can be realized using proposed resonators.

III. DESIGN OF CHIPLESS RFID TAG

A multi-resonator based chipless RFID tag consists of two parts including a multi-resonator circuit exhibiting multiple bits and vertically/horizontally polarized monopole antennas. The multi-resonator circuit determines the frequency codes within a specified frequency band. The frequency band must also be matched with the frequency bands of the monopole antennas. Here, a frequency band between 1.8 and 4 GHz is targeted for the multi-resonator circuit and the monopole antennas.

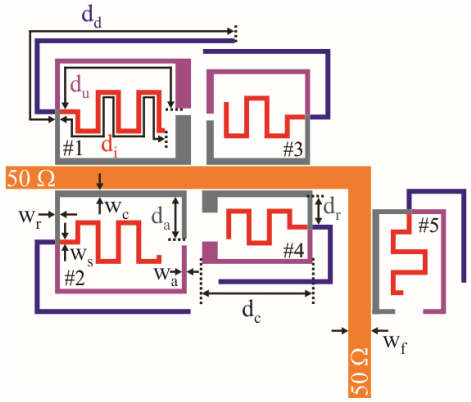

FIGURE 5. Layout of the proposed multi-resonator circuit.

A. DESIGN OF MULTI-RESONATOR CIRCUIT

The proposed multi-resonator circuit consisted of five triple-mode resonators is depicted in Fig. 5. In order to reduce the circuit size and complexity, open stubs with single characteristic impedance are preferred. In order to minimize the inter-resonator coupling, the gaps between the resonators are chosen 1.6 mm corresponding to 2×h (twice the dielectric thickness)

However, it is also possible to use stepped impedance open stubs for each resonator. Since each triple-mode resonator exhibits three resonant frequencies, the proposed circuit has a total of fifteen resonant frequencies. This means that 8^5

TABLE 1. Dimensions of the proposed multi-resonator circuit with five resonators. (all dimensions in mm).

Res. no	1	2	3	4	5
d_i	26.30	22.35	19.40	17.30	15.45
d_d	29.10	24.40	21.05	18.55	16.45
d_u	22.95	22.20	18.50	15.75	15.25
d_a	4.45	4.30	3.90	1.60	1.65
d_c	14.05	13.60	10.70	11.40	10.85
d_r	4.55	4.40	4.00	2.85	2.85
w_c	0.7	0.7	0.7	0.7	0.7
w_r	0.5	0.5	0.5	0.5	0.5
w_s	0.5	0.5	0.5	0.5	0.5
w_a	1.60	0.50	0.75	1.60	0.50

different frequency codes can be obtained. The dimensions of the resonators are determined to target the frequency band between 1.8 and 4 GHz. For this purpose, the theoretical and simulation approaches for a single resonator described in the previous section are considered. Thus, five resonators having almost equal frequency intervals are designed. The designed resonators are then coupled to a bended feeding line. The bended feeding line not only achieves compactness, but also allows for placement of two monopole antennas perpendicular to each other simply. Once the final geometrical configuration is decided, the final dimensions should be determined by optimizing the circuit. The optimizations were carried out using a Full-Wave Electromagnetic Simulator, Sonnet. All dimensions in Fig. 5 are given in Table 1. The coupling gap between the resonators and the feeding line is chosen as 0.15 mm. Frequency responses for four different frequency codes are represented in Fig. 6a. As can be seen from the figure, there are totally 15 bits which can be easily observed. The first three bits in the frequency response are produced by the resonator #1, where the last three bits are generated by the resonator #5. Hence, the bits and resonator numbers are arranged consecutively. Moreover, codes "001", "010" and "100" can be achieved by removing the stubs having lengths of "d_i", "d_u" and "d_o" from each resonator, respectively.

Since the main resonant frequency of the resonator #1 is produced by a half wavelength open loop resonator, the second resonance occurs at about $2f_0$. A security band about 3% of $2f_0$ should be allocated between the highest bit frequency and $2f_0$ to observe the last bit more clearly. Hence, this situation imposes a frequency limitation for the tag. On the other hand, the frequency intervals between the consecutive bits vary between 110 and 140 MHz, so that two more resonators can be added under current conditions. In the simulated response shown in Fig. 6a, the resonance frequencies are 1.98, 2.1, 2.22, 2.34, 2.46, 2.57, 2.71, 2.84, 2.95, 3.08, 3.2, 3.32, 3.43, 3.55, 3.68 GHz. It is also

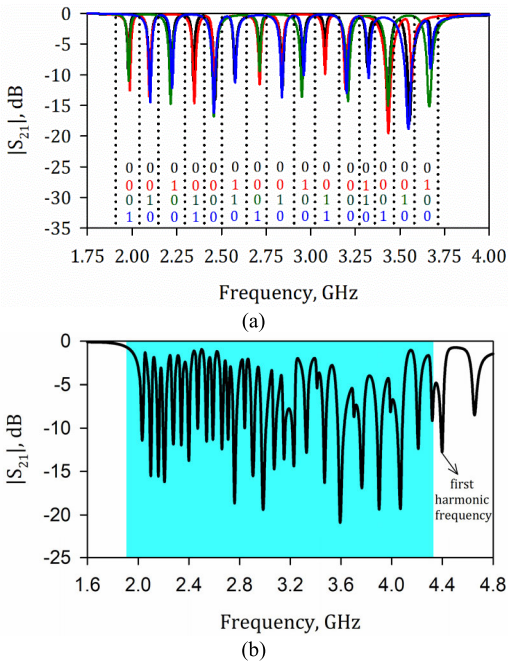

FIGURE 6. Frequency responses of the multiresonator circuit having (a) 15 bits, (b) 30 bits.

possible to increase the number of resonators up to 10 by adjusting the frequency intervals between the bits to about minimum 50 MHz and maximum 140 MHz. To achieve this, an increase in the coupling strength between the resonators and the feeding line is required. The coupling strength can be enhanced by reducing the coupling gap up to about 100 μm or by designing an aperture coupling structure. Fig. 6b illustrates the frequency response of the circuit with a reduced frequency interval. Thus, a more refined fabrication capability or an additional fabrication process is necessary to enhance the coding capacity.

B. MONOPOLE ANTENNA AND CHIPLESS RFID TAG

As mentioned previously, a multi-resonator based chipless RFID tag requires two monopole wideband antennas for receiving the interrogation signal and backscattering. For this purpose, a conventional monopole antenna constructed with a circular patch with a slotted ground plane is used as shown in Fig. 7a [41], [42]. The operating frequencies of the antenna are adjusted by simulations in CST Microwave Studio 2020. The dimensions of the antenna are adjusted to obtain a reflection coefficient lower than -10 dB. In this context, the realized gain is also taken into account within 2-4 GHz which covers the frequencies of the designed multi-resonator circuit. The maximum gain within the mentioned frequency band varies between 2.45 and 4.31 dBi. The simulated reflection coefficient and realized gain are illustrated in Fig. 7b. The dimensions of the proposed wideband monopole antenna are given in Table 2.

The proposed chipless RFID tag is formed by combining a multi-resonator circuit with monopole antennas, as depicted

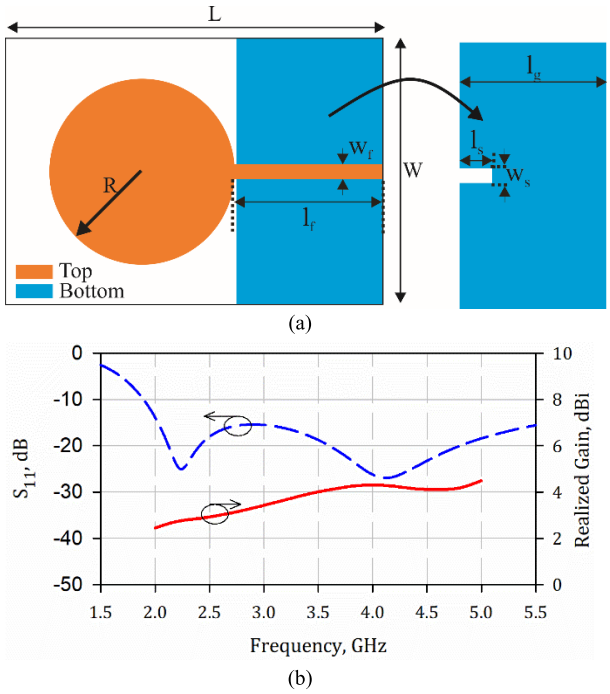

FIGURE 7. a) A monopole wideband antenna for transmitting and receiving parts of the chipless RFID tag, b) simulated frequency responses for reflection coefficient and realized peak gain.

TABLE 2. Dimensions of the monopole antenna.

Parameter	Value (mm)	Parameter	Value (mm)
Total length (L)	57	Total width (W)	43
Patch radius (R)	15	Ground length (l_g)	23.75
Feed line length ($\boldsymbol{l_f}$)	24	Slot length (l_s)	5.25
Feed line width ($\boldsymbol{w_f}$)	2.35	Slot width (w_s)	2.35

in Fig. 8. It should be noted that the monopole antennas are directly integrated into the multi-resonator circuit instead of input and output ports.

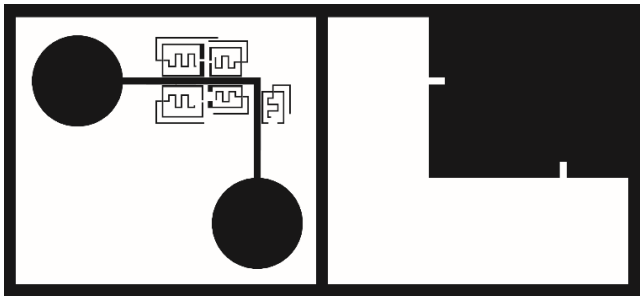

FIGURE 8. Top and bottom views of the chipless RFID tag.

IV. EXPERIMENTAL STUDIES

For demonstration purposes, two chipless RFID tags with different frequency codes have been fabricated and tested.

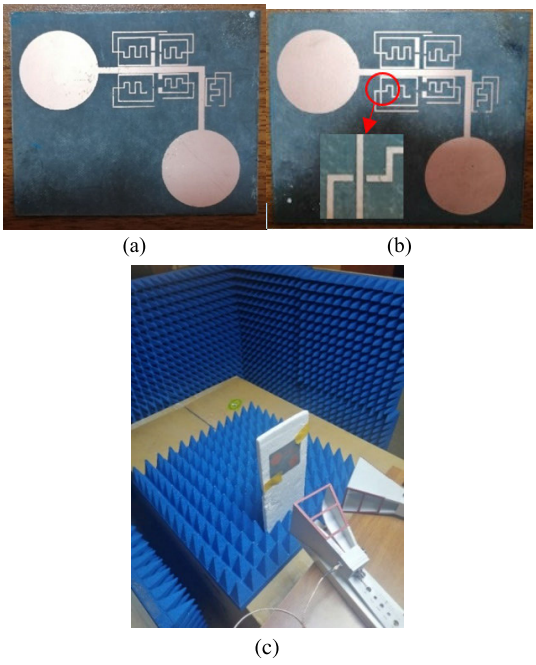

FIGURE 9. Photographs of the fabricated tags for the codes a) 000000000000000, and b) 01010101010101010. c) Measurement setup.

Photographs of the fabricated tags are shown in Figs. 9a and 9b. As can be seen from Fig. 9b, the stubs are separated from the resonators by means of very small gaps. Consequently, to obtain different frequency code, it is possible to remove a stub from the resonator manually, for instance, using a utility knife. Thus, one can attain any frequency code by removing the related stubs depending on the desired code from a tag equipped with all the stubs. A Vector Network Analyzer of Keysight PNA N5222A has been used to measure the transmission coefficients of the tags. Measurements have been realized in a hand-made anechoic chamber. In order to transmit the interrogation signal and receive the backscattered signal, two RF Spin-DRH20E horn antennas have been connected to the Network Analyzer. A sample photo of the test environment is illustrated in Fig. 9c. The electrical lengths of the tags designed with and without monopole antennas are $0.82 \times 0.63\lambda_g^2$ and $0.42 \times 0.27\lambda_g^2$, respectively, where λ_g is the guided wavelength at the first bit frequency.

The measured results of the designed tags are compared with the simulated ones in Fig 10. Fig. 10a illustrates the comparisons for the frequency code "000000000000000". As can be seen from the figure, the measured and simulated results exhibit an excellent agreement in terms of locations of the resonant frequencies. The measured bit frequencies are observed at 1.96, 2.07, 2.21, 2.33, 2.46, 2.57, 2.72, 2.84, 2.96, 3.08, 3.20, 3.31, 3.42, 3.55, 3.68 GHz. Additionally, for the frequency code "010101010101010", the measured and simulated results are compared in Fig. 10b with an excellent agreement. It should be noted that there are seven bits at 1.96, 2.21, 2.45, 2.70, 2.96, 3.21, 3.42, 3.66 GHz

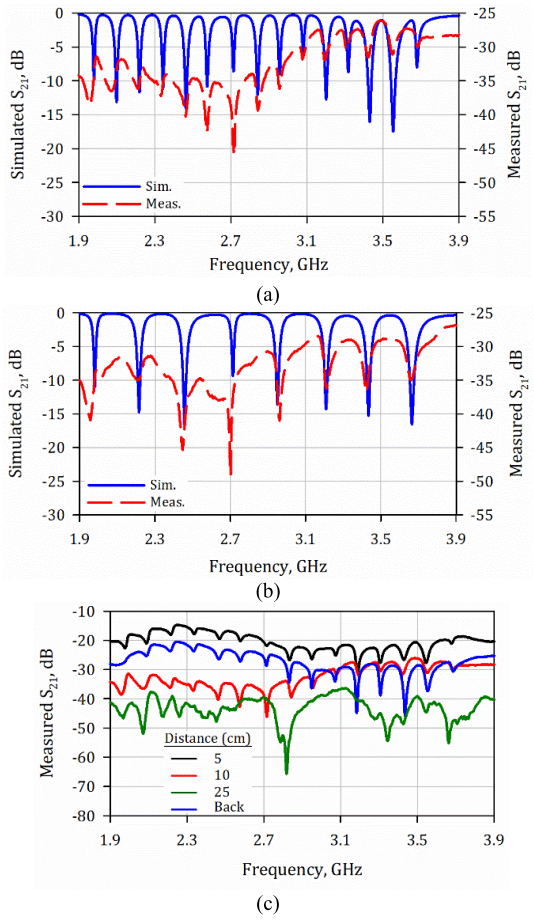

FIGURE 10. Simulated and measured results for the codes a) 000000000000000, b) 010101010101010, c) measured results at different reader distance.

which are the same as the tag having the frequency code "000000000000000". Therefore, the proposed chipless RFID tags may be suitable for item tracking applications because of the excellent agreement between the measured and predicted results. Differences in magnitude between the measured and simulated responses likely arise from the simulation environment since the horn antennas on the reader side and various environmental conditions were not taken into account. The differences are negligible, especially when considering tag performance in terms of the locations of the resonant frequencies. Measurements have also been realized at various tag-reader distances and from the back side of the tag, as depicted in Fig. 10c. As can be seen from the figure, magnitude of the transmission coefficient decreases as the tag moves further away from the reader. It should also be noted that the designed tags operate flawlessly with current monopole antennas when the tag-reader distance is 10 cm. However, disruptions in the measured results can be observed at 25 cm, attributable to environmental factors and antenna performance. The operating distance can be extended by utilizing monopole antennas having better performance. On the other hand, positioning the antennas on both the reader and the tag so that the antennas with the same polarization face each other introduces an angular limitation. Nevertheless, if this angle is maintained, the readability of the frequency code remains, as shown in Figure 10c, even if the back side of the tag is rotated. However, this paper primarily focuses on the observation of a high number of frequency codes based on newly introduced triple-mode resonators.

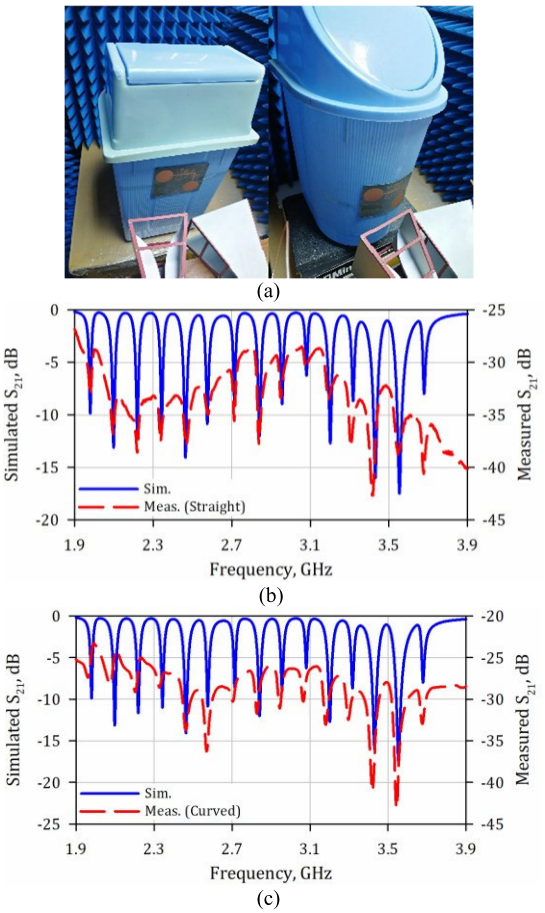

FIGURE 11. Measurements of the proposed tag when attached to a plastic (a) photographs of the measurement setup, (b) measured result for the flat position, (c) measured result for the curved position.

In order to demonstrate the stability of the designed tags, measurements have also been performed under various conditions. The tag has been firstly placed on both flat and curved plastic surfaces, as shown in Fig. 11a. Here, the tag with a frequency code consisting entirely of 0s has been examined. The measured responses under these circumstances are depicted in Figs. 11b and 11c, where all bit frequencies can be clearly observed. Moreover, the proposed tag has been tested when attached to a water bottle, wood, and a metallic surface insulated with styrofoam. The styrofoam has been used to prevent the effect of the metal surface. The test environments for these scenarios are illustrated in Fig. 12a and the corresponding measured responses are shown in Figs. 12b, and 12c, and 12d. Although almost all bits can be clearly observed, some of

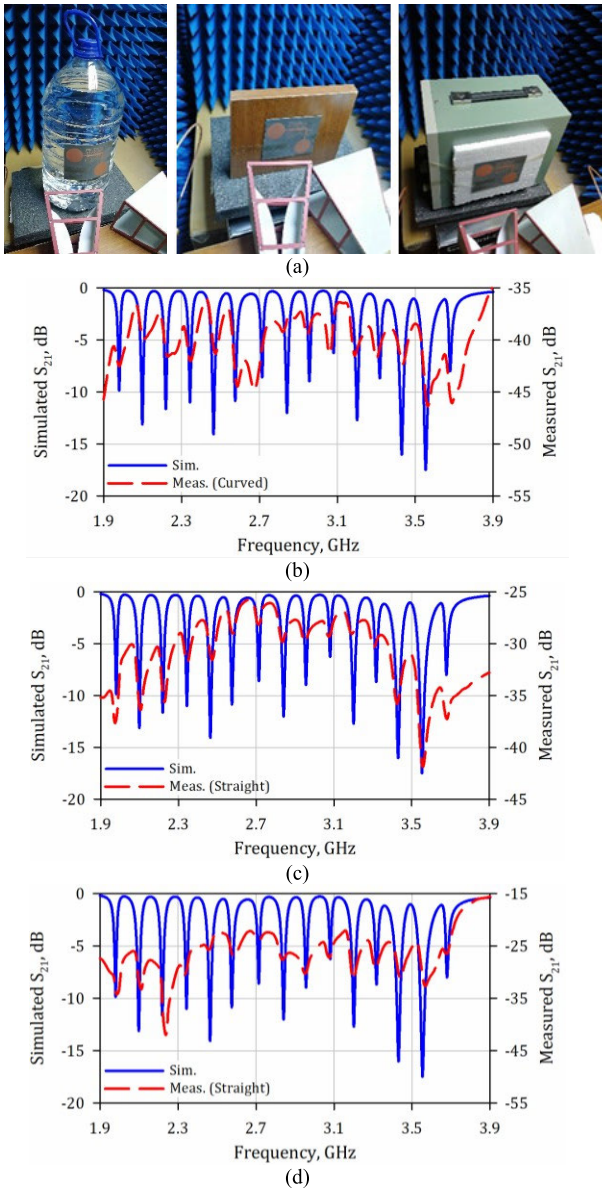

FIGURE 12. Measurements of the proposed tag when attached to different objects (a) photographs of the measurement medium, Measured results for (b) water bottle with curved form, (c) wood with flat form, (d) metallic + styrofoam with straight form.

them suffer from magnitude issues. In order to enhance bit distinguishability, one can consider reference and reference tag measurements as recommended in [43] and [44]. For the reference measurement, no object is placed in front of the horn antennas and the measurement is conducted by only two horn antennas. Then the difference between the responses with and without the tag can be analyzed. This approach is more useful when the tag is in straight position. Reference tag measurements can also improve bit observation. For this purpose, measurement of a tag with no resonators is firstly realized like a calibration. The frequency code in this position will be 1 for all bits. Subsequently, the tag to be measured is replaced instead of the reference tag. By subtracting the results of two measurements, the data can be processed more effectively. During these measurements, time gating should be applied for preventing multiple reflections. Consequently, the designed chipless RFID tags can find many application areas in industry due to their versatile performance capability under various circumstances.

The frequency band in this work has been chosen depending on our fabrication capabilities. Since it overlaps with several communication systems, the current frequency band may be subject to permission due to the regulations on frequency allocations. In this case, one can simply change the frequency band using the mathematical model presented here, and then perform new simulations for the changed frequencies. The design of the tags can be improved in areas such as circuit size, number of resonances, polarization constraints and alignment. In this context, we suggest that researchers consider developing more compact triple mode resonators and monopole antennas. It might be beneficial to use monopole or horn antennas with higher gain and wider beamwidth, thereby potentially reducing issues related to polarization sensitivity and misalignment. Furthermore, a significant limitation for the chipless RFID tags having multi-resonator circuits is the restricted frequency range because of the harmonics of the fundamental resonant frequency. For future work, the fundamental resonant frequencies of the triple-mode resonators can be used after accounting for the resonances introduced by the stubs. Thus, much more resonators can be used to increase the number of resonances.

The proposed chipless RFID tags are compared with similar works in the literature, as given in Table 3. An asymmetrical triple-mode resonator providing eight states is firstly introduced in this work. Since three bits can be easily obtained from a single resonator, there is no need to use three different single-mode resonators. Thus, circuit complexity can be reduced by using less number of resonators. The designed tag offers better bit density and coding variations as compared to the multi-resonator based chipless RFID tags in the literature, with the exception of [25]. Also, the proposed tag exhibits better spectral efficiency performance than other works in the literature except for [17] and [25]. Although the spectral efficiency in [17] is better, its bit density in λ_g and coding variation is quite weak. The bit density and spectral efficiency of the proposed chipless RFID tag are very close to those of [25]. The resonators in [25] are conventional open-loop resonators, so that only one bit and two states can be obtained by a single resonator In contrast, the proposed triple-mode resonator model provides three bits and eight states. Therefore, the proposed tags offer a simpler approach to achieve multiple bits with fewer resonators. For example, while 35 resonators were used to achieve 35-bit frequencies in [25], the same number of bits can be achieved with just 12 resonators in this work. In other words, in order to reach 8^5 frequency codes, only 5 resonators are sufficient in this work, whereas 15 resonators would be required using the coding technique in [25]. A high number of resonators might not only lead to bit observation issues due to the resonator couplings

TABLE 3. State of art.

Ref.	Freq. codes /Res.	Bits /λ_g^2	Freq. codes / λ_g^2	Coding Var.	Spectral Efficiency (Bits/GHz)	Dimensions	BW (GHz)	Type (Method)
[17]	2	23.81	47.62	2^2	10	EA: 0.24 x 0.35 λ_g^2 EA:4 x 5.75 cm^2	0.8-1	U-shaped resonator (flexible)
[18]	8	701.57	1.197 x 10^5	8^4	2.67	EA: 0.181 x 0.189 λ_g^2 EA:2.3 x 2.4 cm^2	1.5-10.5	Improved U-shaped resonator (flexible)
[24]	2	101.39	10383	2^{10}	0.833	EA: 0.375 x 0.263 λ_g^2 EA: 2.28 x 1.6 cm^2	3.6-15.6	Elliptical-shaped resonators/slots (Flexible)
[25]	2	29.869	2.93 x 10^{10}	2^{35}	8.97	1.26 x 0.93 λ_g^2 8.8 x 6.5 cm^2	3.1-7	Spiral resonator
$[27]_1$ $[27]_2$	2 2	22.769 10.199	145.72 1.48 65.28 0.37	2^5 2^5	5 5	EA: 0.61 x 0.36 λ_g^2 EA: 6 x 3.595 cm^2 EA: 0.86 x 0.57 λ_g^2 EA: 15.8 x 5.5 cm^2	2-3	Open stub resonators
[28]	2	8.364	2.86 x 10^3	2^{12}	4	0.95 x 1.51 λ_g^2 6.76 x 10.7 cm^2	3-6	Open stub resonators
[29]	2	10.774 90.91	344.78 1.07 x 10^3	2^8	4	0.99x0.75 λ_g^2 8.0 x 6.0 cm^2 EA: 0.44 x 0.20 λ_g^2 EA: 3.65 x 1.65 cm^2	2-4	Open stub resonators
[30]	3	-	-	3^4	4.32	-	2.9-4.75	Dual-band resonators
[31]	3	5.695	889.567	3^7	4.66	1.65 x 1.49 λ_g^2 4.95 x 4.47 cm^2	6-9	Closed and open loop resonators
[32]	4	-	-	4^4	2.29	-	7.5-11	Modified CSRR
[33]	4	61.76	2.11 x 10^4	4^6	3.64	EA: 0.67 x 0.29 λ_g^2 EA: 2.94 x 1.26 cm^2	5-8.3	Stub-loaded resonators
This Work	**8**	**29.04** **132.28**	**6.343 x 10^4** **2.89 x 10^5**	**8^5**	**8.33**	**0.82 x 0.63 λ_g^2** **8.770 x 6.785 cm^2** **EA: 0.42 x 0.27 λ_g^2** **EA: 4.460 x 2.855 cm^2**	**2-3.8**	**Asymmetrical TMR (flexible)**

Freq.: Frequency, Res.: Resonator, Var.: Variation, BW: Bandwidth, EA: Excluding Antennas.

but also result in a larger tag size. Thus, the proposed work presents an easier approach to control the couplings between the resonators.

V. CONCLUSION

A novel asymmetrical triple-mode resonator for use in the multi-resonator section of chipless RFID tags has been introduced. Depending on the coupling topology of the proposed resonator, eight states can be obtained. Thus, 8^N frequency codes can be achieved by using N triple-mode resonators of different electrical lengths. Five asymmetrical triple-mode resonators operating between 2 and 4 GHz have been designed. They have been coupled to a straight feeding line between the input and output ports to create the multi-resonator circuit. A chipless RFID tag has also been designed by locating two conventional monopole antennas in place of input and output ports. For demonstration purpose, two chipless RFID tags having different frequency codes have been fabricated and tested. The measured results under various test circumstances for both tags have been observed in a very good agreement with the predicted results. This confirms that the proposed tags can be effectively used in both flat and curved configurations on different industrial materials.

Eight state triple-mode resonators are firstly introduced in this paper. They offer a very simple approach to design chipless RFID tags having high number of bits. For straightforward code changes, the tags having all stubs can be used. To achieve a specific code, one simply needs to remove the corresponding stub, a process that can easily be carried out with a utility knife. If necessary, reconnection can be managed by soldering the removed stub back in place or using conductive adhesive tape. However, for optimal performance, it is advisable to design the tag with the desired frequency code from the outset. As a future work, a simple and reliable technique for changing the frequency code can be suggested. Such a technique will make the proposed chipless RFID tags more preferred for the industrial applications.

The performance of these tags can be further enhanced by integrating novel monopole antennas.

REFERENCES

[1] S. Harma, V. P. Plessky, C. S. Hartmann, and W. Steichen, "Z-path SAW RFID tag," *IEEE Trans. Ultrason., Ferroelectr., Freq. Control*, vol. 55, no. 1, pp. 208–213, Jan. 2008.

[2] V. P. Plessky, W. Steichen, S. Harma, and C. S. Hartmann, "PS-1 SAW RFID tag with reduced size," in *Proc. IEEE Ultrason. Symp.*, Apr. 2006, pp. 2389–2392.

[3] S. Harma, V. P. Plessky, X. Li, and P. Hartogh, "Feasibility of ultra-wideband SAW RFID tags meeting FCC rules," *IEEE Trans. Ultrason., Ferroelectr., Freq. Control*, vol. 56, no. 4, pp. 812–820, Apr. 2009.

[4] J. C. Liu and J. H. Yao, "Wireless RF identification system based on SAW," *IEEE Trans. Ind. Electron.*, vol. 55, no. 2, pp. 958–961, Jan. 2008.

[5] S. Harma, W. G. Arthur, C. S. Hartmann, R. G. Maev, and V. P. Plessky, "Inline SAW RFID tag using time position and phase encoding," *IEEE Trans. Ultrason., Ferroelectr., Freq. Control*, vol. 55, no. 8, pp. 1840–1846, Aug. 2008.

[6] A. Chamarti and K. Varahramyan, "Transmission delay line based ID generation circuit for RFID applications," *IEEE Microw. Wireless Compon. Lett.*, vol. 16, no. 11, p. 588–590, Nov. 2006.

[7] M. Schussler, C. Mandel, M. Maasch, A. Giere, and R. Jakoby, "Phase modulation scheme for chipless RFID- and wireless sensor tags," in *Proc. Asia Pacific Microw. Conf.*, Dec. 2009, pp. 229–232.

[8] C. Mandel, M. Schussler, M. Maasch, and R. Jakoby, "A novel passive phase modulator based on LH delay lines for chipless microwave RFID applications," in *IEEE MTT-S Int. Microw. Symp. Dig.*, Sep. 2009, pp. 1–4.

[9] I. Balbin and N. C. Karmakar, "Phase-encoded chipless RFID transponder for large-scale low-cost applications," *IEEE Microw. Wireless Compon. Lett.*, vol. 19, no. 8, pp. 509–511, Aug. 2009.

[10] S. Mukherjee, "Chipless radio frequency identification by remote measurement of complex impedance," in *Proc. Eur. Microw. Conf.*, Oct. 2007, pp. 249–252.

[11] L. Yang, R. Zhang, D. Staiculescu, C. P. Wong, and M. M. Tentzeris, "A novel conformal RFID-enabled module utilizing inkjet-printed antennas and carbon nanotubes for gas-detection applications," *IEEE Antennas Wireless Propag. Lett.*, vol. 8, pp. 653–656, 2009.

[12] J.-L. Jheng, H.-D. Chen, S.-H. Kuo, and H.-W. Yang, "Circularly polarized RFID tag for metal surface mount," in *Proc. Asia Pacific Microw. Conf.*, Dec. 2012, pp. 1037–1039.

[13] T. Athauda and N. C. Karmakar, "The realization of chipless RFID resonator for multiple physical parameter sensing," *IEEE Internet Things J.*, vol. 6, no. 3, pp. 5387–5396, Jun. 2019.

[14] C. Herrojo, J. Mata-Contreras, A. Núñez, F. Paredes, E. Ramon, and F. Martín, "Near-field chipless-RFID system with high data capacity for security and authentication applications," *IEEE Trans. Microw. Theory Techn.*, vol. 65, no. 12, pp. 5298–5308, Dec. 2017.

[15] A. Vena, E. Perret, and S. Tedjini, "Chipless RFID tag using hybrid coding technique," *IEEE Trans. Microw. Theory Techn.*, vol. 59, no. 12, pp. 3356–3364, Dec. 2011.

[16] G. A. Casula and G. Montisci, "A flexible narrowband multiresonator for UHF RFID chipless tag," in *Proc. Microw. Medit. Symp. (MMS)*, May 2022, pp. 1–4.

[17] Z. Wang, Z. Zhang, Y. Hu, H. Zhang, and X. Wang, "Design of a novel compact and flexible chipless RFID tag based on an improved U-shaped resonator," *J. Electromagn. Waves Appl.*, vol. 36, no. 12, pp. 1672–1684, Feb. 2022.

[18] H. Anam, A. Habib, S. I. Jafri, Y. Amin, and H. Tenhunen, "Directly printable frequency signature chipless RFID tag for IoT applications," *Radioengineering*, vol. 26, no. 1, pp. 139–146, Apr. 2017.

[19] V. Sharma, S. Malhotra, and M. Hashmi, "Slot resonator based novel orientation independent chipless RFID tag configurations," *IEEE Sensors J.*, vol. 19, no. 13, pp. 5153–5160, Jul. 2019.

[20] A. A. Awan, M. N. Salimi, M. A. Riaz, H. Shahid, M. A. Asghar, and Y. Amin, "An RFID enabled miniaturized chipless tag for IoT applications," in *Proc. IEEE 23rd Int. Multitopic Conf. (INMIC)*, Nov. 2020, pp. 1–5.

[21] A. T. Khan, M. A. Riaz, H. Shadid, and Y. Amin, "Design of a Cobweb shape chipless RFID tag," *Microw. J.*, vol. 64, p. 90, May 2021.

[22] M. S. Drishyada, D. P. Mishra, and S. K. Behera, "An ultra-wideband chipless RFID tag with L-shaped resonant structures," in *Proc. 2nd Int. Conf. Emerg. Technol. (INCET)*, 2021, pp. 1–5.

[23] I. Jabeen, A. Ejaz, A. Akram, Y. Amin, J. Loo, and H. Tenhunen, "Elliptical slot based polarization insensitive compact and flexible chipless RFID tag," *Int. J. RF Microw. Comput.-Aided Eng.*, vol. 29, no. 11, Nov. 2019, Art. no. e21734.

[24] S. Preradovic, I. Balbin, N. C. Karmakar, and G. F. Swiegers, "Multiresonator-based chipless RFID system for low-cost item tracking," *IEEE Trans. Microw. Theory Techn.*, vol. 57, no. 5, pp. 1411–1419, May 2009.

[25] R. V. Koswatta and N. C. Karmakar, "A novel reader architecture based on UWB chirp signal interrogation for multiresonator-based chipless RFID tag reading," *IEEE Trans. Microw. Theory Techn.*, vol. 60, no. 9, pp. 2925–2933, Sep. 2012.

[26] Y. J. Zhang, R. X. Gao, Y. He, and M. S. Tong, "Effective design of microstrip-line chipless RFID tags based on filter theory," *IEEE Trans. Antennas Propag.*, vol. 67, no. 3, pp. 1428–1436, Mar. 2019.

[27] B. Aslam, M. A. Azam, Y. Amin, J. Loo, and H. Tenhunen, "A high capacity tunable retransmission type frequency coded chipless radio frequency identification system," *Int. J. RF Microw. Comput.-Aided Eng.*, vol. 29, no. 9, Sep. 2019, Art. no. e21855.

[28] C. M. Nijas, R. Dinesh, U. Deepak, A. Rasheed, S. Mridula, K. Vasudevan, and P. Mohanan, "Chipless RFID tag using multiple microstrip open stub resonators," *IEEE Trans. Antennas Propag.*, vol. 60, no. 9, pp. 4429–4432, Sep. 2012.

[29] D. Girbau, J. Lorenzo, A. Lazaro, C. Ferrater, and R. Villarino, "Frequency-coded chipless RFID tag based on dual-band resonators," *IEEE Antennas Wireless Propag. Lett.*, vol. 11, pp. 126–128, 2012.

[30] A. K. Gorur, E. Dogan, G. Ayas, C. Karpuz, and A. Gorur, "Multibit chipless RFID tags based on the transition among closed- and open-loop resonators," *IEEE Trans. Microw. Theory Techn.*, vol. 70, no. 1, pp. 101–111, Jan. 2022.

[31] M. S. Bhuiyan, A. Azad, and N. Karmakar, "Dual-band modified complementary split ring resonator (MCSRR) based multi-resonator circuit for chipless RFID tag," in *Proc. IEEE 8th Int. Conf. Intell. Sensors, Sensor Netw. Inf. Process.*, Melbourne, VIC, Australia, Apr. 2013, pp. 277–281.

[32] W. M. Abdulkawi and A.-F.-A. Sheta, "Four-state coupled-line resonator for chipless RFID tags application," *Electronics*, vol. 8, no. 5, p. 581, May 2019.

[33] R. Dinesh, P. V. Anila, C. M. Nijas, M. Sumi, and P. Mohanan, "Modified open stub multi-resonator based chipless RFID tag," in *Proc. 31th URSI Gen. Assem. Sci. Symp. (URSI GASS)*, Aug. 2014, pp. 1–4.

[34] V. Sharma and M. Hashmi, "Chipless RFID tag based on open-loop resonator," in *Proc. IEEE Asia Pacific Microw. Conf. (APMC)*, Nov. 2017, pp. 543–546.

[35] L. Wang, T. Liu, J. Sidén, and G. Wang, "Design of chipless RFID tag by using miniaturized open-loop resonators," *IEEE Trans. Antennas Propag.*, vol. 66, no. 2, pp. 618–626, Feb. 2018.

[36] M. Hayati, S. Majidifar, and S. N. Sobhani, "Using a hybrid encoding method based on the hexagonal resonators to increase the coding capacity of chipless RFID tags," *Int. J. RF Microw. Comput.-Aided Eng.*, vol. 32, no. 12, Dec. 2022, Art. no. e23474.

[37] A. K. Gorur, E. Dogan, C. Karpuz, and A. Gorur, "Novel multi-resonator circuits for chipless RFID tags using asymmetrical triple-mode resonators," in *Proc. IEEE Int. Conf. RFID (RFID)*, May 2022, pp. 114–119, doi: 10.1109/RFID54732.2022.9795962.

[38] V. K. Tripathi, "Asymmetric coupled transmission lines in an inhomogeneous medium," *IEEE Trans. Microw. Theory Techn.*, vol. MTT-23, no. 9, pp. 734–739, Sep. 1975.

[39] D. M. Pozar, *Microwave Engineering*, 3rd ed. New York, NY, USA: Wiley, 2003, pp. 341–345.

[40] J. S. Hong and M. J. Lancaster, *Microstrip Filters for RF/Microwave Applications*. New York, NY, USA: Wiley, 2001.

[41] J. Jung, W. Choi, and J. Choi, "A small wideband microstrip-fed monopole antenna," *IEEE Microw. Wireless Compon. Lett.*, vol. 15, no. 10, pp. 703–705, Oct. 2005.

[42] Y. Y. Sun, S. W. Cheung, and T. I. Yuk, "Design of a very compact UWB monopole antenna with microstrip-FED," *Microw. Opt. Technol. Lett.*, vol. 55, no. 9, pp. 2232–2236, Sep. 2013.
[43] R. Rezaiesarlak and M. Manteghi, "Short-time matrix pencil method for chipless RFID detection applications," *IEEE Trans. Antennas Propag.*, vol. 61, no. 5, pp. 2801–2806, May 2013.
[44] D. Girbau, A. Lázaro, and R. Villarino, "Passive wireless permittivity sensor based on frequency-coded chipless RFID tags," in *IEEE MTT-S Int. Microw. Symp. Dig.*, Montreal, QC, Canada, Jun. 2012, pp. 1–3.

ENGIN DOGAN (Student Member, IEEE) was born in Aydin, Turkey, in 1993. He received the B.Sc. degree in electrical and electronics engineering from Pamukkale University, Denizli, Turkey, in 2016, and the M.Sc. degree in electrical and electronics engineering from Niğde Ömer Halisdemir University, Niğde, Turkey, in 2019, where he is currently pursuing the Ph.D. degree. He has been a Research Assistant with the Department of Electrical and Electronics Engineering, Niğde Ömer Halisdemir University. His research interests include tunable filters, multiband filters, and chipless RFID tags.

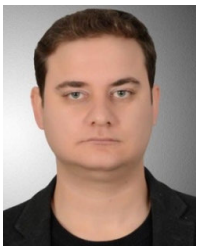

ALI KURSAD GORUR (Member, IEEE) was born in Kayseri, Turkey, in 1986. He received the B.Sc. degree in electrical and electronics engineering from Hacettepe University, Turkey, in 2009, and the M.Sc. and Ph.D. degrees in electrical and electronics engineering from Pamukkale University, Turkey, in 2011 and 2016, respectively. He was with the Department of Electrical and Electronics Engineering, Pamukkale University, as a Research Assistant, from 2011 to 2016. He joined the Department of Electrical and Electronics Engineering, Nevşehir Haci Bektaş Veli University, Turkey, in 2016, as an Assistant Professor, where he has been an Associate Professor, since 2018. His current research interests include tunable/multi-band planar filters, multiplexers, balun bandpass filters for wireless communication systems, and chipless RFID tags.

ADNAN GORUR was born in Hatay, Turkey, in 1961. He received the B.Sc. degree in electronics engineering from Erciyes University, Kayseri, Turkey, in 1983, the M.Sc. degree from Uludağ Üniversitesi, Bursa, Turkey, in 1987, and the Ph.D. degree from Erciyes University, in 1992.

He was appointed as a Research Assistant with the Department of Electronics Engineering, Erciyes University, in July 1984. He became an Assistant Professor, in 1992. In July 1995, he joined the Department of Electrical and Electronics Engineering, Niğde University, Turkey. He became an Associate Professor and a Full Professor with the Department of Electrical and Electronics Engineering, Niğde University, in 1995 and 2005, respectively. He is currently with the Department of Electrical and Electronics Engineering, Niğde Ömer Halisdemir University (formerly Niğde University). He has authored or coauthored over 120 publications. His current research interests include microwave circuits, slow-wave structures, and microstrip filters.